Structure, composition and electrical properties of YSZ films deposited by ultrasonic spray pyrolysis

E. B. Ramírez · A. Huanosta · J. P. Sebastian ·
L. Huerta · A. Ortiz · J. C. Alonso

Abstract Yttria-stabilized zirconia (YSZ) films with different yttria concentrations were prepared by ultrasonic spray pyrolysis on Si substrates at 525 °C, using solutions of zirconium and yttrium acetylacetonates in methanol. The chemical composition, structure and electrical properties of the films were studied by X-ray photoelectron spectroscopy (XPS), X-ray diffraction (XRD), and electrochemical impedance spectroscopy (EIS). XPS measurements show that the Y content in the films increases as the Y precursor in the solution increases. Carbon incorporation was also found in the films, although the concentration of this impurity was reduced as the incorporation of Y increased. XRD spectra show that the $Zr_{1-x}Y_xO_{2-x/2}$ polycrystalline films have the cubic phase of ZrO_2 and fully stabilized 8YSZ (8 at.% Y_2O_3 + 92 at.% ZrO_2), and that their lattice constant increases slightly as the Y content increases. The conductivity of all the as-deposited films as a function of temperature, showed an Arrhenius behavior, and with the exception of the film with the maximum Y content, the activation energies were in the range of 0.98–1.11 eV. The ionic conductivity of one of these films was similar to that measured for a pellet made of the 8YSZ standard powder.

Introduction

Due to its pure ionic conduction, and its high chemical and thermal stability at high temperatures yttrium stabilized zirconium oxide (YSZ) is the predominant solid electrolyte for solid oxide fuel cells (SOFCs) [1–5] and other electrochemical devices such as electrochemical gas sensors [6]. It is well known that yttrium stabilized zirconium oxide in the form of single crystals and/or pellets is fully stabilized in the cubic phase and reaches its maximum ionic conductivity when it contains 8 mol% of Y_2O_3 (8YSZ). At present there are commercial SOFC planar monolithic systems for residential stationary applications and military transport, based on 8YSZ. However, the effect of aging degradation of this material, which consists in the reduction of its electrical conduction when it is operated and/or annealed at 1,000 °C for long time, has become one of the main issues to address in order to assure long-term performance [7–10]. Among the approaches proposed to solve this problem are: the synthesis and investigation of YSZ with lower or higher yttria contents for stabilizing other phases (monoclinic or tetragonal), which do not present the aging effect [7–9], the use of others rare earth oxide dopants for avoiding the aging effect and/or the reduction of the operation temperature of these ceramic electrolytes [10, 11]. In order to reduce the cost and extending the applications of the

E. B. Ramírez · A. Huanosta · L. Huerta ·
A. Ortiz · J. C. Alonso (✉)
Instituto de Investigaciones en Materiales,
Universidad Nacional Autónoma de México,
Ciudad Universitaria, Coyoacan,
Mexico, D.F. 04510, Mexico
e-mail: alonso@servidor.unam.mx

J. P. Sebastian
Centro de Investigación en Energía,
Universidad Nacional Autónoma de México,
Privada Xochicalco s/n, Temixco,
Morelos 62580, Mexico

SOFC systems to the automotive industry, there is also a great interest in reducing the operating temperatures of the solid electrolytes [3–5, 12–19]. Among the approaches directed toward this last purpose, the reduction of the thickness of the YSZ solid electrolyte to a few micrometers or even less than 1 μm seem to be the most attractive. Thus, many recent works have been conducted toward the investigation of the structural and electrical properties of YSZ thin films with yttria contents lower, equal or higher than 8 mol%, deposited by a number of different methods such as; electron beam evaporation [12], reactive DC sputtering [13, 14], magnetron sputtering [15], metal-organic chemical vapor deposition (MOCVD) [16], aerosol-assisted chemical vapor deposition [17], plasma spraying [18], electrostatic spray pyrolysis [19], and pulsed laser ablation [20], among others [5]. In this work, we report a study of the composition, structure, and electrical properties of YSZ thin films with different Yttria contents prepared by ultrasonic spray pyrolysis using acetylacetonate precursors. The ultrasonic spray pyrolysis technique also named pyrosol process, consists in the pyrolysis or thermal CVD process generated by the spraying, at atmospheric pressure, of very fine droplets, on the surface of a hot substrate. We have chosen this deposition technique, because besides having the advantage of being simple and cheap, it allows the deposition of homogeneous metal oxide thin films, endowed with excellent physical properties for several applications [21–25].

Experimental procedure

Sample preparation

The YSZ films were deposited by the ultrasonic spray pyrolysis method, which has been used recently for the preparation of pure zirconia (ZrO_2) thin films [25]. The precursor solution was prepared by dissolving a fixed amount (0.025 M) of zirconium (IV) acetylacetonate [$Zr(acac)_4 = Zr(C_5H_7O_2)_4$] from Sigma–Aldrich Chemicals, in anhydrous methanol. The dopant level of Y_2O_3 was controlled by adding different concentrations of yttrium acetylacetonate hydrate [$Y(acac)_3$ $(H_2O)_x = Y(C_5H_7O_2)_3(H_2O)_x$] (also from Sigma–Aldrich), to the precursor solution. The molar concentration of $Y(acac)_3(H_2O)_x$ was varied at 0.0025 M (YSZ1), 0.005 M (YSZ2), 0.01 M (YSZ3), and 0.02 M (YSZ4). The substrate temperature (T_s) was kept constant at 525 °C, and the carrier gas and director gas flow rate, air in both cases, were fixed at 3.5 and 1.5 l/min, respectively. The deposition time (t_d) was adjusted around 30 min for obtaining films with similar thickness of approximately 1 μm. The substrates used in this work were pyrex glass slices, clear fused quartz slices, and (100) n-type, 0.1–2.0 Ω cm single crystalline silicon slices. All these substrates were ultrasonically cleaned, with trichloroethylene, acetone and methanol. The silicon slices were additionally cleaned with 5% HF solution in order to remove the native oxide.

Sample characterization

The thickness of the films deposited onto pyrex glass was measured with a Sloan Dektac IIA profilometer. For this purpose a small part of the substrate was covered with a cover pyrex glass to form a step during deposition. The thickness of films deposited onto silicon substrates was measured by ellipsometry with a Gaertner 117A ellipsometer using the 632 nm line from a He–Ne laser. In order to make accurate ellipsometric measurements of films thickness, and given that the refractive index of all of them was around 1.9, this parameter was fixed in this value. Under this procedure, both methods, ellipsometry and profilometry, gave similar thickness for films deposited under the same conditions on the different substrates. X-ray diffraction (XRD) spectra were obtained with a Siemens D-500 diffractometer using the CuK$_{\alpha 1}$ wavelength (1.54056 Å). The X-ray source was operated with a voltage of 25 kV and a current of 30 mA, for producing an intense X-ray beam whose incidence angle was 2°. The spectra were obtained for 2θ angles in the range from 5–120° with steps of 0.020°. In order to obtain high quality XRD spectra a long integration or step time (6.9 s) was used. Under these experimental conditions the total time for the acquisition of each spectrum was around 11 h.

The XPS analysis of the films was made by means of a VG Microtech Multilab ESCA 2000 system, equipped with a hemispherical-multichannel detector CLAM4-MDC. The spectra were obtained using the MgK$_\alpha$ ($h\nu$ = 1253.6 eV) X-ray source, operated at 15 kV and 20 mA. The hemispherical sector analyzer was operated in the constant analyzer energy mode, using a pass energy of 50 eV for survey scans and 20 eV for higher resolution spectra of individual core levels used for the quantification purpose.

A tablet of fully stabilized YSZ [8YSZ = $(ZrO_2)_{0.92}$ $(Y_2O_3)_{0.08}$] made from the compression of high purity powder from the NexTech Materials, Ltd. Company, was used as quantitation standard. This standard pellet, was sintered at 950 °C for 8 h inside an oven at atmospheric pressure, and met satisfactorily with the criteria requested for standard samples of having a

known composition, being homogeneous with depth, relatively stable and free of contaminants. Before obtaining the high resolution XPS spectrum for quantitative analysis of each sample, a survey spectrum of its raw surface was obtained in order to check the presence of adsorbed carbon. In most of the cases where surface carbon contamination was found, charge correction was made using the C 1s photoelectron line located at 284.5 as reference. Also, before obtaining the high resolution XPS spectrum, each analyzed sample was cleaned, in situ, with Ar^+ ion sputtering (4.5 keV, $I = 3$ μA, $p = 1 \times 10^{-7}$ mbar) during an interval of 30 s. The analysis of the XPS spectra and data was made using the Spectral Data Processor (SDP) v4.0 software from the χ-XPS International LLC company, which uses for default the RSF from the Scofield table, but allows changing these values for adjusting the composition. The RSF of the O 1s line was kept in its Scofield value meanwhile the RSFs of the Zr 3d and Y 3d lines were adjusted until the correct stoichiometry of the 8YSZ standard was obtained.

Electrical measurements

The electrical conductivity of the YSZ films, as a function of temperature, was measured by applying the electrochemical impedance spectroscopy method to Al/YSZ/Si/Al cells. The Al contacts were thermally evaporated discs of 7 mm in diameter and 200 nm in thickness. Before the evaporation of the Al contact on each silicon substrate, its back was etched with 5% HF solution for removing the native oxide. The geometric constant, $K = l/A$, where l is the thickness of the film and A the electrode surface area, was estimated within ±10% of its average value. For the AC impedance measurements as a function of temperature the electrochemical cells were placed in a normal electrical furnace with controllable temperature. The electrical contact with these cells was made with platinum wires. A chromel–alumel thermocouple placed close to the sample (3–4 mm) was used to detect the equilibrium temperature of the cell for each measurement. The basic equipment for the impedance measurements was a Solartron 1260 frequency response analyzer, operated in the range from 0.1 Hz to 4 MHz. However, in order to check the reproducibility of the measurements, some of the cells were also measured using a Hewllet-Packard HP4192A automatic impedance analyzer. Also, as a procedure of calibration and for the sake of comparison, the AC impedance of a electrochemical cell prepared with a pellet of 1 mm in thickness of the 8YSZ standard powder, sandwiched in between gold electrodes of 7 mm in diameter, was

measured in both equipments, and the obtained results were similar. The range of temperatures investigated in the AC impedance experiments was 200–450 °C for most of the YSZ films. In this case the maximum temperature was limited, in order to avoid spurious effects such as: the oxidation of the Al electrodes and/or the silicon substrate, and/or the diffusion of Al atoms toward the silicon substrate. In the case of the 8YSZ pellet with Au electrodes, the AC impedance measurements were made in the temperature range from 300 °C to 650 °C.

Results and discussion

Structure and composition

Figure 1 shows the X-ray diffraction patterns of YSZ films deposited with different Y_2O_3 content, which is
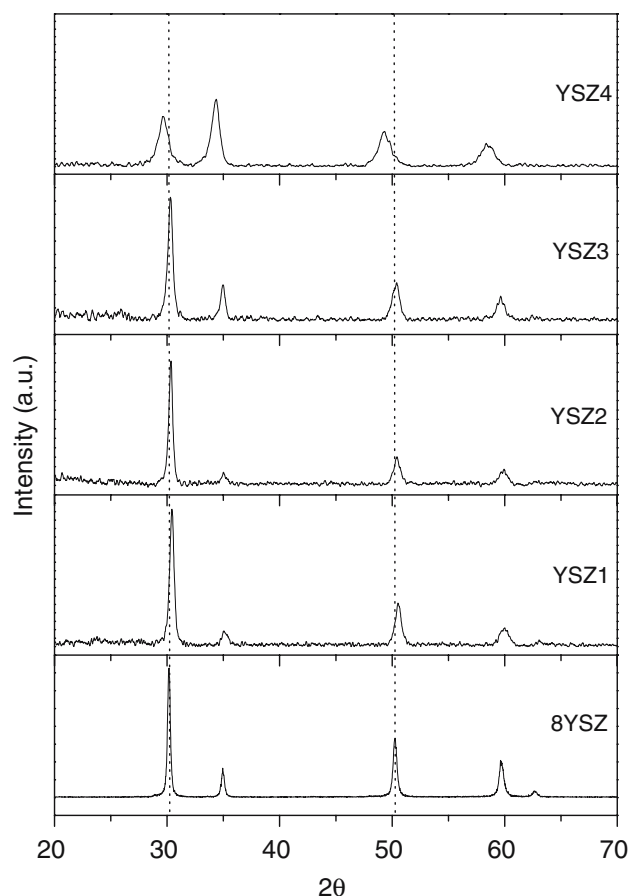
Fig. 1 XRD patterns of the 8YSZ standard and YSZ films prepared by the pyrosol process using different $Y(acac)_3(H_2O)_x$ molarities; 0.0025 M (YSZ1), 0.005 M (YSZ2), 0.01 M (YSZ3), and 0.02 M (YSZ4). The substrate temperature (T_s) was kept constant at 525 °C

proportional to the molar fraction of $Y(acac)_3(H_2O)_x$ in the start solution, as it is shown below. For the sake of comparison the XRD pattern of the 8YSZ standard is also shown in this figure (bottom spectrum). Table 1 summarizes the position of the four main XRD peaks for the analyzed samples, as well as those indicated in the JCPDS cards for the possible crystalline phases present in these samples. As Table 1 shows, the location (2θ) of the main diffraction peaks for the standard corresponds quite well to the cubic phase of fully stabilized 8YSZ compound. The angular positions of the main diffraction peaks for the YSZ1, YSZ2 and YSZ3 films, correspond to the cubic phase of ZrO_2 and fully stabilized YSZ. The small shift of these peaks toward lower angles, as the Y content increases, indicates that the lattice constant of the cubic phase of the $Zr_{1-x}Y_xO_{2-x/2}$ films suffers a slight increment with Y content. On the other hand, the positions of the main XRD peaks of the YSZ4 film, which has the maximum Y_2O_3 content, are shifted toward that corresponding to the Cubic Y_2O_3 phase. The average crystallite-size in the films was determined using the Voigt function method for the calculation of the integral breadth of the broadened X-ray diffraction line profiles, which enables the separation of both, microstrain and grain size contributions to the line broadening [26, 27]. Under this approach the line profile of one component (the first diffraction peak in our case) is convoluted using Lorentzian (Cauchy) and Gaussian functions, and the crystallite size D is given by; $D = \lambda/\beta_L\cos\theta$, where β_L is the integral breadth of the Lorentzian function, λ is the wavelength of the X-ray source, and θ the Bragg angle of the peak used in the determination. Table 1 shows that the grain size in the deposited films first increases slightly from 27.2 nm to 32.7 nm as the Y content is slightly increased, but then, for further increase in the Y content, the grain size decreases until 10.7 nm. The grain size in the

8YSZ tablet is 40.2 nm. Using the ratio of the integrated intensity of the background to the intensity of the main peak for each spectrum (Relative Intensity Ratio method), a rough estimation of the amorphous to crystalline phase ratio (a/c ratio) was made. As Table 1 shows, the percentage of amorphous phase in the films is relatively low and increases with the Y content.

Figure 2 shows the XPS survey spectra of the YSZ films prepared with different Y_2O_3 contents, along with the spectrum of the 8YSZ standard. All the spectra exhibit the peaks associated to Zr and Y, such as: Zr 3d (183.0 eV), Zr $3p_{3/2}$ (333.5 eV), Zr $3p_{1/2}$ (347 eV), Zr 3s (434 eV), Y 3d (158.5 eV), Y $3p_{3/2}$ (301.5 eV), Y $3p_{1/2}$ (313.5 eV), and the O 1s (530.5 eV) peak. It is worth mentioning that the binding energies of these peaks were practically the same for all the spectra. The binding energies of the Zr 3d and Y 3d peaks indicate that zirconium and yttrium atoms in the films are mostly bonded to oxygen [28–30]. A visual inspect of the spectra shows that the relative intensity of the Y peaks increase as the molarity of yttrium acetylacetonate in the precursor solution increases. A small peak of C 1s (285 eV) appears in the films with the lowest Y content, indicating some carbon contamination, but this peak decreases as the yttrium content increases. The O 1s peak and the main peaks of Zr and Y (Zr 3d and Y 3d), were chosen for quantification of the composition of the 8YSZ standard. The RSF value of the O 1s peak was kept constant at its Scofield value (2.93), meanwhile the RSF values for the Zr 3d and Y 3d peaks were changed and adjusted to values of 7.96 and 8.3, respectively, for reproducing the composition of this standard. Then, using these RSF values, the composition of the deposited YSZ films was determined. The atomic percentages of Zr, Y, O and C in all the films are shown in Table 2. As expected, the yttrium content increases as the molarity of

Table 1 2θ positions of the main XRD peaks, grain sizes and rough estimation of the a/c phase ratios for all the as-deposited YSZ prepared by the pyrosol process with different Y content, and the 8YSZ standard
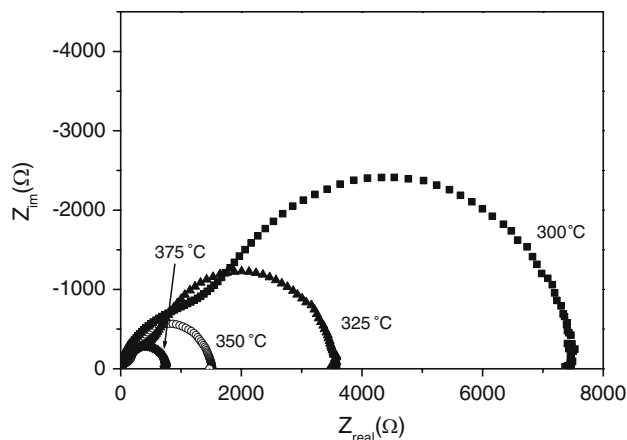
Sample	1st peak	2nd peak	3rd peak	4th peak	Grain size (nm)	a/c ratio
YSZ1	30.44°	35.15°	50.52°	60°	27.2	0.035
YSZ2	30.34°	35.02°	50.41°	59.96°	32.7	0.040
YSZ3	30.31°	34.96°	50.39°	59.66°	21.8	0.053
YSZ4	29.66°	34.35°	49.30°	58.67°	10.7	0.064
8YSZ standard	30.18°	34.94°	50.26°	59.76°	40.2	–
JCPDS cards						
Cubic $(ZrO_2)_{0.92}(Y_2O_3)_{0.08}$	30.109°	34.896°	50.179°	59.649°		
Cubic ZrO_2	30.509°	35.193°	50.686°	60.337°		
Cubic Y_2O_3	29.409°	34.037°	48.887°	58.073°		
Monoclinic ZrO_2	28.175°	31.468°	34.16°	50.116°		
Tetragonal ZrO_2	29.831	34.023	34.855°	49.51°		

For the sake of comparison, the data from the JCPDS cards are also shown
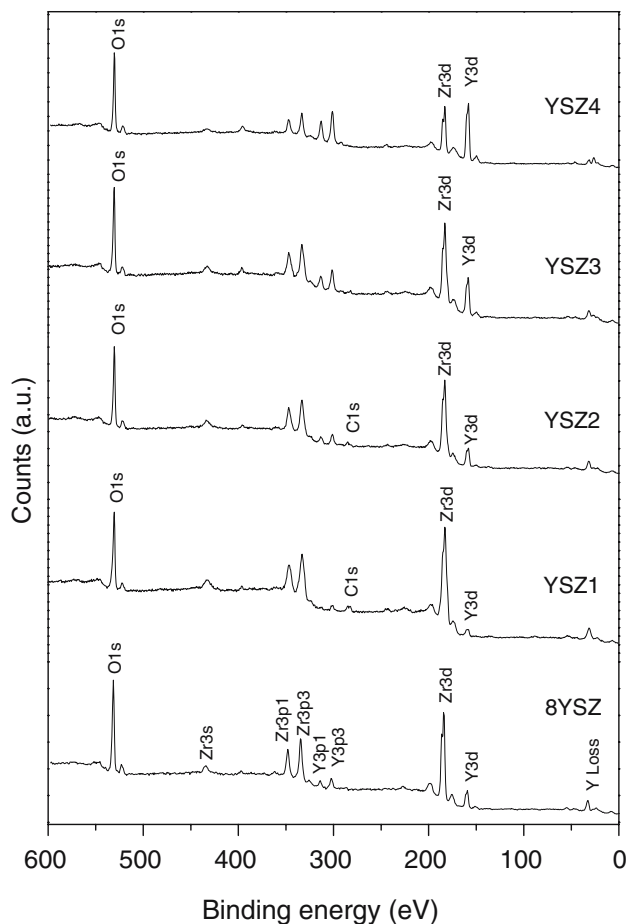
Fig. 2 Typical XPS survey spectra of YSZ films prepared by the pyrosol process using different $Y(acac)_3(H_2O)_x$ molarities; 0.0025 M (YSZ1), 0.005 M (YSZ2), 0.01 M (YSZ3), and 0.02 M (YSZ4). The bottom spectrum is for the 8YSZ standard

Fig. 3 Typical impedance diagrams at 300, 325, 350, and 375 °C for the YSZ2 film

for the decrease in the C content as the Y content increases, is not well understood at present. However, it could be associated with some reactions between oxygen atoms of the water molecules coming from the $Y(acac)_3(H_2O)_x$ precursor and carbon atoms of the acetylacetonates, which can extract carbon through the formation of volatile CO_2 [23, 31].

Electrical conductivity

Figure 3 shows typical impedance diagrams in the complex plane (Nyquist plots) for the YSZ2 film, at different equilibrium temperatures. The Nyquist plots for the other films were similar, as well as its behavior with temperature. Two overlapping and a little depressed semicircles are clearly seen in most of the Nyquist plots, which suggest the presence of resistances and capacitances associated with the electrolyte bulk (grain), the grain boundary and electrode processes. Although there are several microscopic model and/or approaches for simulating the impedance spectra, we chose the equivalent circuit approach for the simulation a data analysis, because it is more popular in the study of solid ionic materials, and it is also more simple and practical when there is interest in knowing the magnitude of the ionic conductivity rather than

$Y(acac)_3(H_2O)_x$ in the precursor solution increases. These results are quite consistent with the trends observed in the X-ray diffraction patterns of correspondent samples. For example, the X-ray diffraction pattern of the film with the smallest Y content (2.6 at.%), almost corresponds with that of cubic ZrO_2, meanwhile the diffraction pattern of the film with the highest Y content (19.7 at.%), which is in fact higher than the Zr content (17.3 at.%), corresponds more closely with that of cubic Y_2O_3 phase. The reason

Table 2 XPS composition results and electrical properties for the 8YSZ standard and all the as-deposited YSZ films

Sample	Zr (at.%)	Y (at.%)	O (at.%)	C (at.%)	E_a (eV)	A (Ω/cm/K)	σ (Ω/cm) $T = 400$ °C
YSZ1	34.6	2.3	51.8	11.36	1.11	7.65×10^3	5.43×10^{-8}
YSZ2	21.3	6.1	63.1	9.5	1.00	1.47×10^4	7.24×10^{-7}
YSZ3	27.7	10.9	57.4	4.0	0.98	7.44×10^5	4.89×10^{-6}
YSZ4	17.3	19.7	63.1	0	0.35	2.11×10^{-2}	7.42×10^{-8}
8YSZ standard	29.1	5.1	65.8	0	1.00	1.3×10^5	5.93×10^{-6}

RSF values used: O 1s (2.93), Zr 3d (7.96), Y 3d (8.3), C 1s (1.39)

knowing the detailed conduction mechanisms [12, 18, 20, 32]. Thus, all the impedance diagrams were simulated, using the Zview program, by a series network of two or three sub-circuits, each one consisting of one resistor and one capacitor in parallel. From this simulation the total resistance, R, was determined for each impedance diagram and then the conductivity of each film as a function of temperature was calculated from the expression $\sigma = K/R$, where K is the geometric factor. It is worth mentioning that the contribution of the Si substrate to the total resistance can be neglected because it is various orders of magnitude lower. On the other hand, the aluminum electrodes kept its high conductivity in the oxidizing environment (air), only up to 450 °C. Above this temperature the aluminum electrodes started oxidizing, as it was confirmed by the increase in the impedance of the electrochemical cell.

Figure 4 show the plots of log (σT) versus $10^3/kT$ for all the as-deposited films and for the 8YSZ pellet. As can be seen, in the range of temperatures investigated (200–450 °C for the films, and 300–650 °C for the pellet), all the plots adjust quite well to straight lines, which indicates that the conductivity for all these samples can be expressed in the form of the Arrhenius relationship: $\sigma T = A \exp(-E_a/kT)$, where E_a is the activation energy for ion migration, A is the pre-exponetial factor, k is the Boltzman constant and T is the temperature in degree Kelvin. Using the least squares method for the linear fitting of the Arrhenius plots, the values of the activation energies and pre-exponential factors shown in Table 2 were obtained. Table 2 also shows the conductivity of the films at 400 °C along with the conductivity of the 8YSZ pellet at the same temperature. As can be seen from this table, the activation energy of the films (YSZ1–YSZ3) suffers a slight decrease from 1.11 eV to 0.98 eV, meanwhile the pre-exponential factors and conductivity increase in two orders of magnitude as the yttrium content increases from 2.3 to 10.9 at.%. On the other hand the film (YSZ4) with the highest yttrium content (19.7 at.%) has a very low activation energy (0.35 eV) and pre-exponential factor, which give rise again to a low conductivity. The increase in the conductivity of the YSZ films (YSZ1, YSZ2, YSZ3), as the Y content increases from its lowest value (2.3 at.%) is quite expected, since it is well known that the substitution of trivalent Y^{3+} cations for the tetravalent Zr^{+4} cation of the host ZrO_2 lattice, not only stabilizes the cubic fluorite structure but also creates a large concentration of oxygen vacancies by charge compensation, which give rise to a higher oxygen ion mobility [1]. As the XPS composition results show, these films contain

carbon, and the fact that the atomic concentration of this impurity decreases as the yttrium content increases, seems to be indicative that the incorporation of carbon deteriorates the conductivity, perhaps through the formation of covalent bonds with Zr atoms, which would have the effect of decreasing the concentration of oxygen vacancies and/or mobile O^{-2} ions. The decrease in the conductivity of the YSZ4 film prepared with excess of Y, can be explained as a result of a change in the host material, from ZrO_2 to Y_2O_3, which is a material with a lower intrinsic ionic conductivity. This explanation is supported by the fact that this film contains more yttrium than zirconium atoms, as Table 2 shows, and also by the fact that its XRD pattern corresponds more to the Y_2O_3 cubic phase than the ZrO_2 cubic phase.

The data of Table 2 and the visual comparison of the plots of Fig. 4 show that the YSZ3 film has electrical characteristics similar to those of the 8YSZ pellet. These results and the fact that the conductivity of this as deposited film is similar or higher than that of films deposited or sintered at higher temperatures by other techniques such as electron beam evaporation [12], DC sputtering and slip casting [14], and aerosol-assisted chemical vapor deposition [17] is encouraging for applying these films as electrolyte in SOFCs. In spite of this, the conductivity of our best film (YSZ3) is still lower than the conductivity of similar films deposited by other techniques such as plasma spray [18], and it must be improved for its efficient application in second-generation solid oxide fuel cells. As it was mentioned before, it is possible that the conductivity of our films is limited by the incorporation of carbon, so, it is feasible to improve the conductivity in the near future by eliminating this impurity through
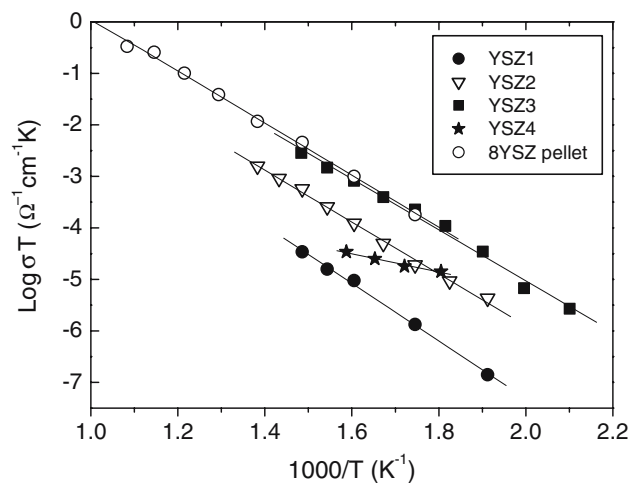
Fig. 4 Arrhenius plots of specific conductivity for the YSZ1–YSZ4 films and the 8YSZ standard

the addition of small and controlled amounts of water to the start solution [23, 31].

Conclusions

YSZ thin films with a thickness of ~1 μm have been deposited on silicon and glass substrates (at 525 °C) by the pyrosol process, using metal acetylacetonates diluted in anhydrous methanol as precursor materials. The results showed that the concentration of Y in the deposited films is proportional to the molarity of yttrium acetylacetonate in the start solution and that the Y content has an important effect on the structure and electrical properties of the films. YSZ Films with Y concentrations lower or equal than 10.9 at.%, develop the cubic fluorite structure with average grain size of about 27.2 nm, which has a slight dependence with Y content. These films also contain carbon whose concentration decreases as the Y content increases. The conductivity of as-deposited films with Y concentrations lower or equal than 10.9 at.%, as a function of temperature follows an Arrhenius behavior with similar activation energy (0.98–1.1 eV) but with a pre-exponential factor that increases significantly as the Y content increases. In spite that the film with an Y content of 10.9 at.%, contain 4.0 at.% of carbon, its structure and ionic conductivity were very similar to those of the 8YSZ standard bulk material.

On the other hand, the film deposited with the highest Y molarity used in this work, result with more Y incorporated (19.7 at.%) than Zr (17.3 at.%) and consequently have a structure close to the cubic phase of Y_2O_3, with a smaller grain size (10.7 nm). Although this film does not contain carbon, its ionic conductivity is strongly deteriorated.

The best results concerning to the ionic conductivity of the our as-deposited YSZ films, encourages further research work in order to optimize and improve the application of the pyrosol process in the preparation of thin films of solid oxide electrolytes.

References

1. Minh NQ (1993) J Am Ceram Soc 76:563
2. Kozhukharov V, Brashkova N, Ivanova M, Carda J, Machkova M (2002) Bol Soc Esp Cerám Vidrio 41:471
3. Mori T, Drennan J, Lee JH, Li JG, Ikegami T (2002) Solid State Ionics 154–155:529
4. Ralph JM, Schoeller AC, M. Krumpelt (2001) J Mater Sci 36:1161
5. Will J, Mitterdofer A, Kleinlogel C, Perednis D, Gauckler LJ (2000) Solid State Ionics 131:79
6. Di Bartolomeo E, Kaabbuathong N, Grilli ML, Traversa E (2004) Solid State Ionics 171:173
7. Bartolomé JF, Montero I, Díaz M, López-Esteban S, Moya JS, Deville S, Gremillard L, Chevalier J, Fantozzi G (2004) J Am Ceram Soc 87:2282
8. Haering C, Roosen A, Schichl H (2005) Solid State Ionics 176:253
9. Bao W, Zhu W, Zhu G, Gao J, Meng G (2005) Solid State Ionics 176:669
10. Yamamoto O, Arati Y, Takeda Y, Imanishi N, Mizutani Y, Kawai M, Nakmura Y (1995) Solid State Ionics 79:137
11. Boulćh F, Dessemond L, Djurado E (2002) Solid State Ionics 154–155:143
12. Hartmanová M, Thurzo I, Jergel M, Bartos J, Kadlec F, Zelezný V, Tunega D, Kundracik F, Chromik S, Brunel M (1998) J Mater Sci 33:969
13. Wanzenberg E, Tietz F, Panjan P, Stöver D (2003) Solid State Ionics 159:1
14. Wanzenberg E, Tietz F, Kek D, Panjan P, Stöver D (2003) Solid State Ionics 164:121
15. Ruddell DE, Stoner BR, Thompson JY (2003) Thin Sold Films 445:14
16. Chevalier S, Kilo M, Borchardt G, Larpin JP (2003) Appl Surf Sci 205:188
17. Meng G, Song H, Dong Q, Peng D (2004) Solid State Ionics 175:29
18. Chiodelli G, Magistris A, Scagliotti M, Parmigiani F (1988) J Mater Sci 23:1159
19. Perednis D, Gaucker LJ (2004) Solid State Ionics 166:229
20. Kosacki I, Rouleau CM, Becher PF, Bentley J, Lowndes DH (2005) Solid State Ionics 176:1319
21. Langlet M, Joubert JC (1993) In: Rao CNR (ed) Chemistry of advanced materials. Blackwell Scientific Publications, Oxford, pp 55–79
22. Ortiz A, Alonso JC, Pankov V, Andrade E, Urbiola C (2001) J Electrochem Soc 148:F26
23. Ortiz A, Alonso JC (2002) J Mater Sci Mater Electron 13:7
24. Catañeda L, Alonso JC, Ortiz A, Andrade E, Saniger JM, Bañuelos JG (2002) Mater Chem Phys 77:938
25. Ortiz A, Alonso JC, Haro-Ponoatowski E (2005) J Electron Mater 34:150
26. Keijser TH, Langford JI, Mittemeijer EJ, Vogels ABP (1982) J Appl Cryst 15:308
27. Valvoda V (1992) In: Eckertová L, Ruzicka T (eds) Diagnostics and applications of thin films. IOP Publishing, London, pp 115–132
28. Zhang NL, Song ZT, Wan Q, Shen QW, Lin CL (2002) Appl Surf Sci 202:126
29. Wang SJ, Ong CK (2002) Appl Phys Lett 80:2541
30. Hughes AE, Sexton BA (1989) J Mater Sci 24:1057
31. Nasibulin AG, Shurgina LI, Kauppinen EI (2005) Colloid J 67:1
32. Jiang SP, Love JG, Badwal SPS (1997) In: Nowotny J, Sorrell CC (eds) Key Engineering Materials, vol 125–126. Trans Tech Publications, Switzerland, pp 133–162